Liquid Crystals

ISSN: 0267-8292 (Print) 1366-5855 (Online) Journal homepage: http://www.tandfonline.com/loi/tlct20

Dye-integrated cholesteric photonic luminescent solar concentrator

Andrea L. Rodarte, Fredy Cisneros, Linda S. Hirst & Sayantani Ghosh

To cite this article: Andrea L. Rodarte, Fredy Cisneros, Linda S. Hirst & Sayantani Ghosh (2014) Dye-integrated cholesteric photonic luminescent solar concentrator, Liquid Crystals, 41:10, 1442-1447, DOI: 10.1080/02678292.2014.924163

To link to this article: http://dx.doi.org/10.1080/02678292.2014.924163

Liquid Crystals, 2014
Vol. 41, No. 10, 1442–1447, http://dx.doi.org/10.1080/02678292.2014.924163

Taylor & Francis
Taylor & Francis Group

Dye-integrated cholesteric photonic luminescent solar concentrator

Andrea L. Rodarte, Fredy Cisneros, Linda S. Hirst* and Sayantani Ghosh*

School of Natural Sciences, University of California, Merced, CA, USA

(*Received 28 April 2014; accepted 11 May 2014*)

We have developed organic dye-integrated thin-film liquid crystalline photonic luminescent solar concentrators (LSCs), where the chirality of the liquid crystal (LC) results in the formation of a one-dimensional photonic cavity. By varying the different LSC parameters, including dye concentration, spectral position of the photonic band-gap and the LC phase, and by using spectroscopic and electrical characterisation, we have systematically studied the effects of self-absorption, incident absorption and confinement of down-converted emission on optical efficiency. Our results demonstrate that the efficiency of our LSCs is significantly enhanced in the LC phase when the photonic band-gap is at long wavelengths (>600 nm), overcoming associated low incident absorption and higher self-absorption. We reach the significant conclusion that focusing on improving the confinement of dye-emitted photons, rather than on increasing incident absorption, is a more promising route to enhancing thin-film LC-based LSC performance.

Keywords: luminescent solar concentrators; optical devices; cholesteric; fluorescent dye

1. Introduction

First designed and studied in the 1970s,[1,2] luminescent solar concentrators (LSCs) have recently regained prominence, although with a modified focus. At the time of their initial invention, the most advantageous premise of these devices was that they used smaller amounts of expensive silicon (Si) in comparison with the traditional solar panels.[3] Now, with Si being much cheaper, LSCs have lost that advantage. However, they have other unique properties, including flexibility,[4,5] and functionality that covers both direct and diffuse lighting, removing the need for tracking mechanisms.[6] This makes them ideal candidates for incorporation in a typical city, where buildings have small footprints but large vertical areas.[7,8] The usual design of an LSC consists of a transparent glass or polymer sheet, doped with a fluorescent material. The fluorophores are chosen to optimise broadband solar absorption and emission (quantum yield), minimise self-absorption and provide good spectral overlap with the electric band-gap of the photovolatic material located at the edges for the final photocurrent generation.[9–13] While the choice of fluorophores varies between a wide range of organic dyes, semiconducting polymers and quantum dots, the host is usually an inert matrix.[14–17] Recently, photonic luminescent solar concentrators (PLSCs) have been developed, in which photonic crystal films are externally applied to an LSC to assist in photon management [18,19] by reducing escape cone losses. In this configuration, the photonic films act as reflectors across a particular spectral band, enhancing photon confinement within the device. An alternate strategy for creating a PLSC is to use the photonic material itself as the concentrating slab – a concept that was recently explored theoretically.[20] In this work, we have developed a PLSC consisting of a slab of cholesteric liquid crystal (CLC) material. Organic dye molecules are dispersed in the cholesteric film, forming an active fluid one-dimensional photonic cavity with a tunable stop band.

A schematic representation of our LSC is shown in Figure 1(a). In the chiral CLC phase, the rod-like component molecules have short-range orientational order [21] and in our device, are arranged with their rotational axis perpendicular to the top and bottom glass surfaces (planar alignment). The distance over which the LC molecules complete a 360° orientational rotation about this axis is denoted the 'pitch' of the material. The CLC phase exhibits a spectral band-gap when the direction of incident radiation (bold green arrows) is parallel with the chiral rotational axis, therefore acting as a one-dimensional photonic cavity.[22] One critical variation between typical photonic band-gap materials and this CLC-based one is that here the band-gap is 50% reflective [23–25] as circularly polarised light matching the handedness of the CLC will propagate through the device. An important advantage of using a CLC in this application is that the spectral position of the band-gap can be easily tuned by varying the chirality of the CLC. The dye molecules dispersed in the CLC matrix

*Corresponding authors. Emails: sghosh@ucmerced.edu (Sayantani Ghosh); lhirst@ucmerced.edu (Linda S. Hirst)

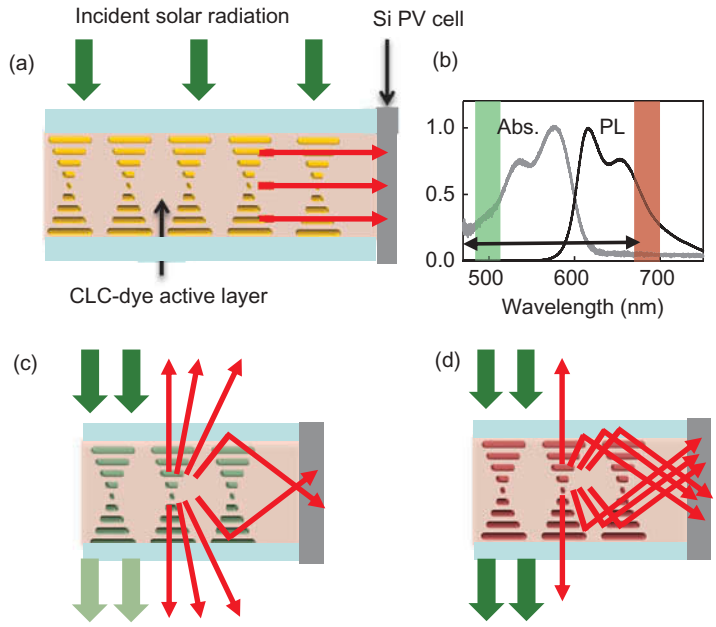

Figure 1. (a) Schematic representation of CLC-dye-based LSC; (b) Normalised absorption and photoluminescence (PL) of the dye. The double headed arrow denotes the spectral range over which we vary the photonic band-gaps for different LSCs; (c) Schematic representation of LSC *A* showing high absorption of incident radiation, but low confinement of emitted light; (d) Schematic representation of LSC *B* showing low absorption but high confinement of emitted light.

absorb the incident light and the down-converted emission is wave-guided to the edges by total internal reflection (red arrows) where it generates photocurrent in the attached Si PV cells. Normalised absorption and emission spectra of the dye used (Lumogen F Red 300) are shown in Figure 1(b). Figure 1(c) and (d) shows schematics representing the expected differences in device behaviour as the cholesteric band-gap changes. A photonic band-gap centred on the absorption band will trap incident light more effectively (Figure 1(c)) but be unable to confine the emission, while a band-gap resonant with the emission will not be a very effective absorber, though it will allow better confinement of emitted photons that otherwise would escape the LSC.

Lumogen F Red 300 has a planar molecular structure and is therefore expected to exhibit some tendency to align with the cholesteric host molecules. In a recent publication,[17] this effect was shown to enhance the output current of an LSC using a homeotropically aligned polymerisable nematic LC host slab with the dye Coumarin 6. In that device configuration, the dye molecules aligned with the LC and emitted preferentially to the edges of the device, reducing escape cone losses. In our device configuration, the planar configuration of the cholesteric molecules may produce a dye anisotropy that will act to reduce device efficiency if significant dye alignment occurs. However, such losses could be offset by the action of the reflection band.

In this study, we design a dye-incorporated composite liquid crystalline LSC where we track optimal performance not only by varying dye concentration and LC phase, but also by tuning the photonic band-gap over the spectral region indicated in Figure 1(b) (double arrows), which allows us to address the contributions of device absorption, surface losses and self-absorption systematically.

2. Results and discussion

The CLC used in the LSC devices is prepared using varying concentrations of the nematic LC, 4′-pentyl′4-biphenylcarbonitrile (5CB, Sigma Aldrich) mixed with the cholesteric LC, cholesteryl oleyl carbonate (COC, Sigma Aldrich). These room temperature LC materials are used as proof of concept only, and ultimately, the device would require LC materials with a significantly higher clearing point. Varying the proportions by weight of COC in 5CB allows us to tune the photonic band-gap of the CLC. Liquid crystal A contains 68% wt COC to create a photonic band-gap centred around 500 nm. Liquid crystal B contains 48% wt COC to create a photonic band-gap centred around 690 nm. The mixtures are sonicated in a heated bath above the clearing point for both component materials (43°C) for 1 h to achieve a homogeneous mixture. The dye, Lumogen F Red 300 (BASF), dissolved in toluene, is then added to the LC mixture to create concentrations of 4 mM,

9 mM and 14 mM composite LSCs. These are again sonicated in a heated bath for 1 h and subsequently removed to a 50°C vacuum oven and maintained at 635 Torr overnight in order to remove residual solvent. The samples are then sonicated one more time in a heated bath for 1 h prior to preparing the LSC.

For LSC production, 1 mm-thick clean glass slides are treated with a 1 wt% aqueous polyvinyl alcohol (Sigma Aldrich) solution on the active side. Once the slide is dry, the surface is rubbed with velvet to create a planar alignment layer for the CLC. Prepared glass is then glued together using Mylar spacers to create cells approximately 10 μm thick. Finished LSCs have an active area of 20 × 20 mm and are filled via capillary action while maintaining the isotropic phase and subsequently cooled at a rate of 1°C/minute to a final temperature of 25°C on a Linkam LTS350 hot-stage. Formation of the CLC phase is verified by using polarised optical microscopy to observe the characteristic birefringence texture. Once the cholesteric phase has been verified, we use transmission and reflection data to calculate the absorptance of the LSC. These are measured using a Motic-150 halogen 150 W cold light source. The LSC is mounted on an Instec HCS302 hot and cold stage to maintain a constant 30°C temperature for cholesteric phase measurements and 40°C for isotropic phase measurements. Spectra collected by an Acton 300i spectrometer are dispersed onto a thermoelectrically cooled CCD with a spectral resolution of ~0.18 nm. The absorptance calculated for a 4 mM dye concentration in LSCs *A* (band-gap centred at 500 nm) and *B* (690 nm) is shown in Figure 2(a and b), for both the CLC (black, 30°C) and the isotropic (grey, 40°C) phases. In LSC *A*, where the band-gap overlaps the dye absorption spectrum, the CLC phase shows a clear increase in absorptance compared to the isotropic phase. In LSC *B*, there is a peak in the absorptance, but that is a result of the incident white light trapped by the LSC and does not enhance the dye properties. For this reason, for photocurrent measurements shown in Figure 5, we use a low-pass filter that cuts off at 650 nm in the incident path. In addition to absorptance, Figure 2 also compares the emission from the edge of the LSCs. While both LSCs have higher-intensity edge emission in the cholesteric phase than the isotropic, the increase is much larger in LSC *B*, as expected. In all other LSCs with intermediate photonic band-gaps, similar enhancements are seen in absorption and/or emission in the CLC phase when compared to the isotropic.

Apart from incident absorption and emission, self-absorption is an additional factor that impacts the efficiency of any LSC. It is the result of spectral overlap between the absorption and emission bands (Figure 1(b)), which causes reabsorption of emitted photons by the dye molecules themselves. Self-absorption worsens with length of travel of the emitted photons and manifests itself as reduced emission intensity and overall spectral redshift in the light that finally reaches the edges.[26] To assess the role of concentration and photonic band-gap position in self-absorption in our cells, we perform spatially resolved spectral measurements. The cell is mounted on a motorised translation stage and coupled to an optical fibre at the edge. A collimated incident beam is used to excite a 2-mm-diameter spot on the cell. The distance between the excitation point and the collection fibre at the edge is continuously varied by translating the LSC.

Figure 3(a and b) shows the dye emission spectra at different distances between the excitation and collection spots for LSCs *A* and *B*, at 4 mM dye concentration. The emission is spectrally bimodal and as the distance between excitation and collection increases, we observe the weight distribution shifting from lower (labelled 'Peak 1') to higher (labelled 'Peak 2') wavelengths, accompanied by a decrease in intensity, both typical signatures of self-absorption by the dye molecules. Dye concentration is an additional parameter that influences self-absorption considerably. In Figure 3(c and d), we show the spectral weight of each peak for 2.5 mm and 10 mm separations for two different concentrations obtained from fits to spectral curves as shown in Figure 3(a and b). At 4 mM, (Figure 3(c)), the spectral shift is

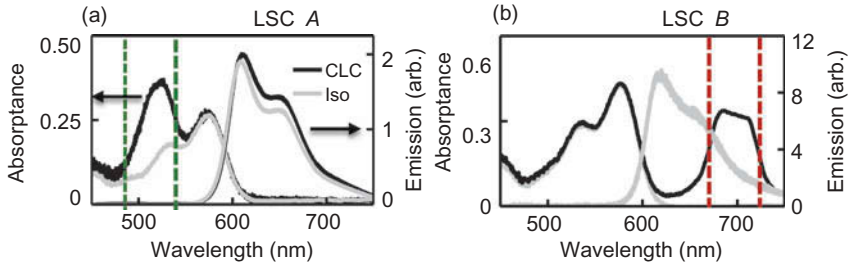

Figure 2. (colour online) Dye absorption and emission spectra in isotropic (grey) and CLC (black) phases for stop band-gaps centred on (a) 500 nm – overlapping dye absorption and (b) 690 nm – overlapping dye emission. The dashed lines indicate the spectral positions of the band-gaps.

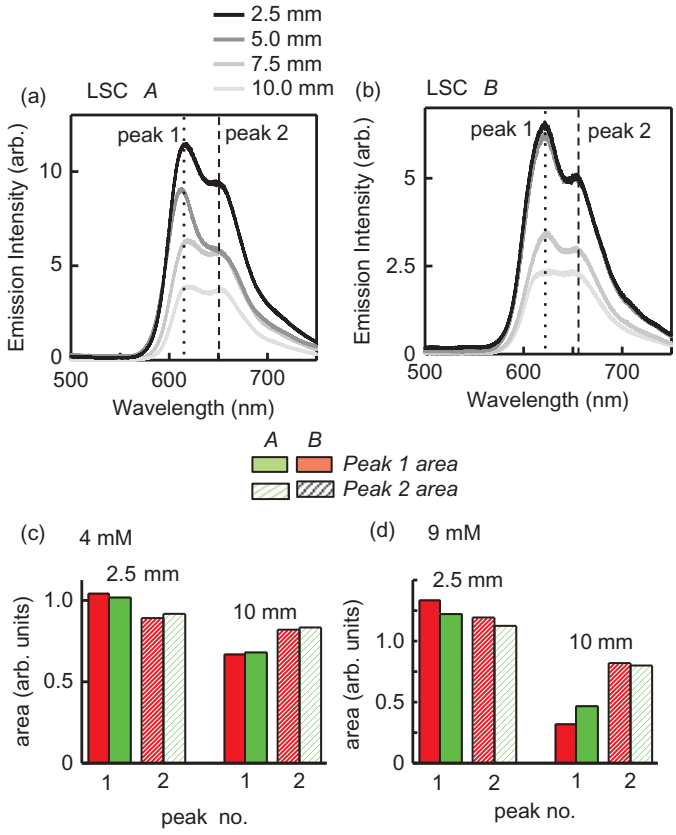

Figure 3. (colour online) Evaluation of self-absorption losses using pump-probe technique. The emission spectra are shown for different pump-probe separations for (a) LSC *A* and (b) LSC *B*. Dotted and dashed lines indicate the spectral positions of the two peaks, designated Peak 1 and Peak 2. The comparative weights of each peak for the two devices with pump-probe separations of 2.5 and 10 mm are shown for (c) 4 mM and (d) 9 mM dye concentrations.

very similar in both LSCs, as is the overall intensity drop (ranging from 22% to 23%). At 9 mM of dye, differences show up. For LSC *A*, 15.2% of the lower peak weight shifts to the higher one, but for LSC *B* this shift is 23%, which would imply greater self-absorption. However, the weight shift does not correlate to overall decrease in intensity. The intensity loss for LSC *A* is 55% for 9 mM, while for LSC *B* it is only 46%. This is unusual in typical LSCs, where greater relative spectral weight redshift almost always indicates increased self-absorption and corresponding loss of yield.[27] We speculate that most likely LSC *B* does have more self-absorption, but this effect is masked by the higher degree of confinement due to the photonic band-gap.

After these fundamental optical characterisations, we move onto photocurrent measurements. These are carried out by mounting a Si photovoltaic cell with an active area of 2 × 30 mm to the edge of the LSC using index-matched adhesive (Norland 78). To control the phase of the CLC, the LSCs are then mounted on an Instec temperature stage with a reflective white backing layer between the LSC and the stage. The LSC is maintained in the CLC phase (30°C) for 6 minutes and the photocurrent, (I_{LSC}) is measured every 10 seconds. The variation in I_{LSC} with time is shown in Figure 4. Incident light is blocked periodically, indicated by breaks in the data. At the end of the 360 seconds, the LSC is heated to the isotropic phase (40°C) and data are taken for another 360 seconds. Figure 4(a) shows the normalised I_{LSC} for a well-aligned cell (transmission image in Figure 4(b)) in which the current drops 2% after being heated to the isotropic phase. The observed current jump immediately after 360 seconds in Figure 4(a) is a result of the phase change at that point. By comparison, I_{LSC} of a poorly aligned LSC in which many defects disturb the planar alignment, as verified by the defect-rich disordered transmission image in Figure 4(d), is shown in Figure 4(c). Poorly aligned LSCs showed a less-consistent I_{LSC} that increases when the LSC is heated into the isotropic phase. Clearly, the presence of a photonic band-gap in a well-aligned LSC leads to improved performance.

Next, we investigate how this improved performance varies with the spectral position of the photonic band-gap, with particular focus on whether absorption or emission plays the greater role in device

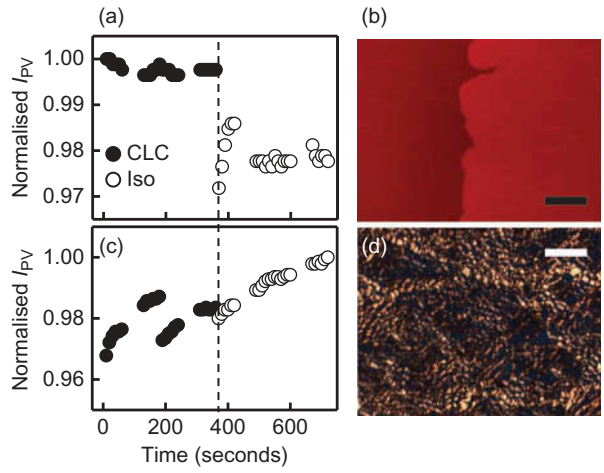

Figure 4. (colour online) Photocurrent as a function of time for (a) a well-aligned device with a photonic band-gap centred on 690 nm (b) and a poorly aligned control LSC. (c, d) Transmission images of the well- and poorly aligned LSCs, respectively. The dashed line indicates the time when LSCs were heated to the isotropic phase. Scale bar is 50 μm.

efficiency. We define the absorption efficiency for different LSCs as the total light absorbed by the LSC divided by the total light incident upon the LSC:

$$\eta_{\mathrm{Abs}} = \int_{\lambda} I(\lambda) A_{\mathrm{bs}}(\lambda) d\lambda \Big/ \int_{\lambda} I(\lambda) d\lambda, \tag{1}$$

where $I(\lambda)$ is the light incident upon the LSC and $A_{\mathrm{bs}}(\lambda)$ is the absorptance, calculated from measured absorption spectra, such as in Figure 2. The absorptance for different LSCs is normalised to the peak of the dye absorption to remove effects of concentration or thickness. Optical efficiency is defined as:

$$\eta_{\mathrm{OPT}} = (I_{\mathrm{LSC}} \times A_{\mathrm{PV}})/(I_{\mathrm{PV}} \times A_{\mathrm{LSC}}), \tag{2}$$

where I_{LSC} is the current generated by the LSC attached to the PV cell, I_{PV} is the short circuit current of the bare PV cell, A_{LSC} is the area of the top of the LSC and A_{PV} is the active area of the PV cell. The ratio of $A_{\mathrm{LSC}}/A_{\mathrm{PV}}$ is referred to as the geometric factor for the LSC. We calculate η_{Abs} and η_{OPT} for all our LSCs in both the CLC and isotropic phases and observe a maximum η_{OPT} of ~12% in LSC *B*. However, here we show the percentage change for each of the efficiencies between the two LC phases in Figure 5(a) and (b). For most LSCs, η_{Abs} is higher in the CLC phase, and, as expected, this improvement diminishes as the photonic band-gap shifts to higher wavelengths. The LSCs with a band-gap >650 nm show barely any change between the isotropic and the CLC phase. The optical efficiency, on the other hand, shows the opposite trend. We observe that despite exhibiting higher absorption in the CLC phase, LSC with band-gaps centred in the 500–600 nm range do not have a corresponding increase in η_{OPT}. Instead, the most consistent increase in η_{OPT} comes from the LSCs with photonic band-gaps centred above 650 nm, even though those devices have lower η_{Abs} in the CLC phase and additionally suffer from higher self-absorption. The effect of dye concentration on device efficiency shows the most dilute LSC performs the best. With increasing concentration self-absorption gets worse (as seen in Figure 3) and usually that is compensated by higher incident absorption. In these LSCs even that is not the case, which is most likely due to the CLC phase (and in effect, the band-gap) being less uniform and well-defined as more dye is added to the LC.

3. Conclusions

Our studies establish the important result that when using a photonic band-gap type material to enhance performance of an LSC, matching its spectral stop band to maximise emission confinement is more advantageous than trying to enhance incident absorption. In addition, the use of a thin-film composite material that

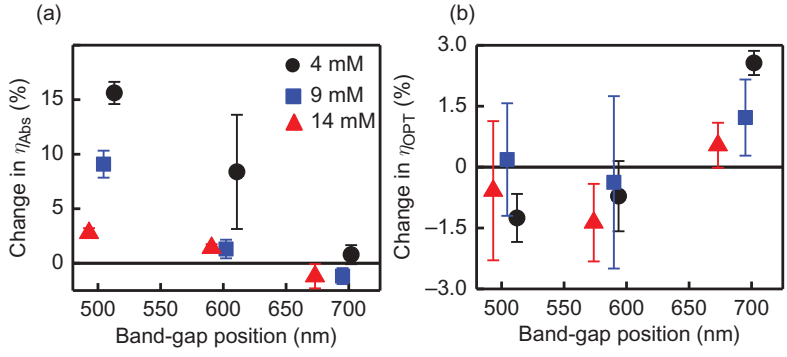

Figure 5. (colour online) (a) Change in absorption efficiency (η_{Abs}) and (b) change in optical efficiency (η_{OPT}) from CLC to isotropic phase.

performs the dual functionality of providing both the down conversion of absorbed photons and the photonic band-gap-related confinement of emitted photons makes our devices viable candidates for solution-based processing of LSCs that can be easily incorporated as thin-films onto windows and other similar surfaces.

Funding

We would like to acknowledge the support from NSF [grant number DMR-1056860].

References

[1] Weber WH, Lambe J. Luminescent greenhouse collector for solar radiation. Appl Opt. 1976;15:2299. doi:10.1364/AO.15.002299
[2] Goetzberger A, Greube W. Solar energy conversion with fluorescent collectors. Appl Phys. 1977;14:123–139. doi:10.1007/BF00883080
[3] Batchelder JS, Zewail AH, Cole T. Luminescent solar concentrators. 1: theory of operation and techniques for performance evaluation. Appl Opt. 1979;18:3090. doi:10.1364/AO.18.003090
[4] Yoon J, Li L, Semichaevsky AV, Ryu JH, Johnson HT, Nuzzo RG, Rogers JA. Flexible concentrator photovoltaics based on microscale silicon solar cells embedded in luminescent waveguides. Nat Commun. 2011;2:343. doi:10.1038/ncomms1318
[5] Chou C-H, Chuang J-K, Chen F-C. High-performance flexible waveguiding photovoltaics. Sci Rep. 2013;3. doi:10.1038/srep02244
[6] Slooff LH, Bende EE, Burgers AR, Budel T, Pravettoni M, Kenny RP, Dunlop ED, Büchtemann A. A luminescent solar concentrator with 7.1% power conversion efficiency. Phys Status Solidi RRL. 2008;2:257–259. doi:10.1002/pssr.200802186
[7] Chemisana D. Building integrated concentrating photovoltaics: a review. Renew Sust Energ Rev. 2011;15:603–611. doi:10.1016/j.rser.2010.07.017
[8] Wang C, Hirst LS, Winston R. editors. Optical design and efficiency improvement for organic luminescent solar concentrators. Proc SPIE. 2011;8124:812400.
[9] Rowan BC, Wilson LR, Richards BS. Advanced material concepts for luminescent solar concentrators. IEEE J Sel Top Quantum Electron. 2008;14:1312–1322. doi:10.1109/JSTQE.2008.920282
[10] Reisfeld R. New developments in luminescence for solar energy utilization. Opt Mater. 2010;32:850–856. doi:10.1016/j.optmat.2010.04.034
[11] Lü W, Kamiya I, Ichida M, Ando H. Temperature dependence of electronic energy transfer in PbS quantum dot films. Appl Phys Lett. 2009;95:083102. doi:10.1063/1.3213349
[12] Shcherbatyuk GV, Inman RH, Wang C, Winston R, Ghosh S. Viability of using near infrared PbS quantum dots as active materials in luminescent solar concentrators. Appl Phys Lett. 2010;96:191901. doi:10.1063/1.3422485
[13] Inman RH, Shcherbatyuk GV, Medvedko D, Gopinathan A, Ghosh S. Cylindrical luminescent solar concentrators with near-infrared quantum dots. Opt Express. 2011;19:24308. doi:10.1364/OE.19.024308
[14] Bailey ST, Lokey GE, Hanes MS, Shearer JDM, McLafferty JB, Beaumont GT, Baseler TT, Layhue JM, Broussard DR, Zhang Y, Wittmershaus BP. Optimized excitation energy transfer in a three-dye luminescent solar concentrator. Sol Energy Mater Sol Cells. 2007;91:67–75. doi:10.1016/j.solmat.2006.07.011
[15] Krumer Z, Pera SJ, van Dijk-Moes RJ, Zhao Y, de Brouwer AF, Groeneveld E, van Sark WG, Schropp RE, de Mello Donegá C, van Sark WG, Schropp RE, de Mello Donegá C. Tackling self-absorption in luminescent solar concentrators with type-II colloidal quantum dots. Sol Energy Mater Sol Cells. 2013;111:57–65. doi:10.1016/j.solmat.2012.12.028
[16] Maggioni G, Campagnaro A, Carturan S, Quaranta A. Dye-doped parylene-based thin film materials: application to luminescent solar concentrators. Sol Energy Mater Sol Cells. 2013;108:27–37. doi:10.1016/j.solmat.2012.08.009
[17] Mulder CL, Reusswig PD, Velázquez A, Kim H, Rotschild C, Baldo M. Dye alignment in luminescent solar concentrators: I. Vertical alignment for improved waveguide coupling. Opt Express. 2010;18:A79. doi:10.1364/OE.18.000A79
[18] Wehrspohn RB, Üpping J. 3D photonic crystals for photon management in solar cells. J Opt. 2012;14:024003. doi:10.1088/2040-8978/14/2/024003
[19] Peters M, Goldschmidt JC, Löper P, Bläsi B, Gombert A. The effect of photonic structures on the light guiding efficiency of fluorescent concentrators. J Appl Phys. 2009;105:014909. doi:10.1063/1.2996081
[20] Gutmann J, Peters M, Bläsi B, Hermle M, Gombert A, Zappe H, Goldschmidt JC. Electromagnetic simulations of a photonic luminescent solar concentrator. Opt Express. 2012;20:A157. doi:10.1364/OE.20.00A157
[21] Hirst LS. Fundamentals of soft matter science. Boca Raton (FL): CRC Press; 2012.
[22] Rodarte AL, Gray C, Hirst LS, Ghosh S. Spectral and polarization modulation of quantum dot emission in a one-dimensional liquid crystal photonic cavity. Phys Rev B. 2012;85:035430. doi:10.1103/PhysRevB.85.035430
[23] Timofeev IV, Arkhipkin VG, Vetrov SY, Zyryanov VY, Lee W. Enhanced light absorption with a cholesteric liquid crystal layer. Opt Mater Express. 2013;3:496. doi:10.1364/OME.3.000496
[24] Debije MG, Van M-P, Verbunt PPC, Kastelijn MJ, van der Blom RHL, Broer DJ, Bastiaansen CWM. Effect on the output of a luminescent solar concentrator on application of organic wavelength-selective mirrors. Appl Opt. 2010;49:745. doi:10.1364/AO.49.000745
[25] Giebink NC, Wiederrecht GP, Wasielewski MR. Resonance-shifting to circumvent reabsorption loss in luminescent solar concentrators. Nat Photonics. 2011;5:694–701. doi:10.1038/nphoton.2011.236
[26] Sholin V, Olson JD, Carter S. Semiconducting polymers and quantum dots in luminescent solar concentrators for solar energy harvesting. J Appl Phys. 2007;101:123114. doi:10.1063/1.2748350
[27] Sansregret J, Drake JM, Thomas WRL, Lesiecki ML. Light transport in planar luminescent solar concentrators: the role of DCM self-absorption. Appl Opt. 1983;22:573. doi:10.1364/AO.22.000573